

Experimental
Communication

Cite

Zdrazilova L, Hansikova H, Gnaiger E (2021)
Comparable respiratory activity in attached and suspended fibroblasts.
MitoFit Preprints 2021.7.
doi:10.26124/mitofit:2021-0007

Author contributions

LZ and EG designed the work; LZ collected and analyzed data, LZ and EG wrote the article, all authors contributed to the final version of the manuscript.

Conflicts of interest

EG is founder and CEO of Oroboros Instruments, Innsbruck, Austria.

Received 2021-09-21

Accepted 2021-09-21

Online 2021-09-21

MitoFit Preprints 2021.7
doi:10.26124/mitofit:2021-0007




Data availability

Original files are available Open Access at Zenodo repository:
[10.5281/zenodo.5518059](https://zenodo.org/record/5518059)

Keywords

attached cells, ace
suspended cells, sce
fibroblasts
high-resolution
respirometry, HRR
Oroboros O2k
Seahorse Bioanalyzer
XF24
ROUTINE respiration, *R*
LEAK respiration, *L*

Comparable respiratory activity in attached and suspended human fibroblasts

 Lucie Zdrazilova¹,  Hana Hansíková¹,
 Erich Gnaiger²

¹Department of Pediatrics and Inherited Metabolic Disorders, First Faculty of Medicine, Charles University and General Hospital in Prague, Czechia;

²Oroboros Instruments, Innsbruck, Austria

*Corresponding author: erich.gnaiger@orooboros.at

MitoFit Preprints 2021.7. doi:10.26124/mitofit:2021-0007

Abstract

Measurement of oxygen consumption of cultured cells is widely used for diagnosis of mitochondrial diseases, drug testing, biotechnology, and toxicology. Fibroblasts are cultured in monolayers, but physiological measurements are carried out in suspended or attached cells. We address the question whether respiration differs in attached and suspended cells using multiwell respirometry (Agilent Seahorse XF24) and high-resolution respirometry (Oroboros O2k), respectively. Respiration of human dermal fibroblasts measured in culture medium was baseline-corrected for residual oxygen consumption and expressed as oxygen flow per cell.

No differences were observed in ROUTINE respiration of living cells and LEAK respiration obtained after inhibition of ATP synthase by oligomycin. Multiple steps of uncoupler titrations in the O2k allowed for evaluation of maximum electron transfer capacity, which was higher than respiration obtained in the XF24 due to a limitation to two uncoupler titrations.

electron transfer
capacity, *E*
residual oxygen
consumption, *Rox*
bioenergetic cluster
analysis, BCA

Quantitative evaluation of respiration measured in different platforms revealed that short-term suspension of fibroblasts did not affect respiratory activity and coupling control. Consistent results obtained with different platforms provide a test for reproducibility and allow for building an extended respirometric database.

1. Introduction

Studies of cells attached in a monolayer or suspended in the medium have wide-ranging applications and implications. These include metabolic profiling (Ladzins et al 1980), substrate diffusion (Pofit et al 1977), cell morphology and rheology (Harrison et al 1979), macrophage adherence (Pofit et al 1977), suspension culture as mimetic of circulating tumor cells (Park et al 2017), metastatic potential (Park et al 2017), therapeutic cell reimplantation, and cell culture biotechnology and pharmacology (Shen et al 2019).

The structure of cells growing in culture changes from the attached to suspended state. After blebbing, cells undergo membrane reorganization and attain a spherical shape to prevent membrane loss (Harrison et al 1979). In rabbit lung macrophages, transport of lysine and adenosine across the plasma membrane is faster in suspended compared to adherent cells (Pofit et al 1977). Moreover, mouse macrophages oxidize glucose six-times faster in suspension than monolayers (Ladzins et al 1980). Suspending anchorage-dependent fibroblasts results in an abrupt drop of mRNA production, while protein synthesis declines slowly but extensively, and recovery of protein synthesis requires surface contact (Benecke et al 1978; Farmer et al 1978). This raises the physiological question, whether cell respiration differs in suspended versus attached fibroblasts. Stimulatory or suppressive effects may be exerted on aerobic ATP demand and consequently respiration may be regulated differently in suspended and attached states.

The Seahorse XF Analyzer (Agilent, US) is designed for studying respiration of attached cells (ace), whereas the Oroboros O2k (Oroboros Instruments, Austria) is optimized for high-resolution respirometry with suspended cells (sce). In the present study we used these platforms to investigate respiration in attached and suspended fibroblasts applying comparable and standardized protocols for monitoring respiratory activity in living cells under near-physiological conditions. Specific titration steps in the protocol disrupt the physiological control of respiration, which then allows for instrumental comparison of performance of the two platforms. Respiratory activity was normalized per cell and expressed in identical SI units for quantitative comparison of the data. The experimental period of suspended cells was limited to less than one hour. The respiratory activity of suspended and attached cells was not distinguishable during such short time intervals. Comparative studies provide the basis for extending databases of

cellular respiration by including critically evaluated results obtained with different platforms.

2. Materials and methods

2.1. Reagents

DMEM5030, Carbonyl cyanide 4-(trifluoromethoxy)phenylhydrazone (FCCP, C2920-10MG), oligomycin(O4876-5MG), antimycin A (A8674-25MG), rotenone (R8875-1G), and glutamine (G7513-100mL) were purchased from Sigma Aldrich. Trypsin-ethylenediaminetetraacetic acid EDTA 10x (XC-T1717/100) and antibiotics-antimycotics 100X (XC-A4110/100) were obtained from Biosera, Dulbecco's modified Eagle's medium (DMEM, P04-04510) from Pan Biotech, fetal bovine serum (SV30160.03) from HyClone, and XF Calibrant Solution 100840-000 from Agilent.

2.2. The instruments

The Seahorse XF Analyzer (Agilent, Santa Clara, US) provides multi-well plate analysis of two processes in real time, (1) oxygen consumption rate (OCR) as an indicator of cell respiration, and (2) extracellular acidification rate largely dependent on glycolytic processes. Cellular O₂ consumption causes changes in the concentration of dissolved dioxygen O₂ in so called 'transient microchambers'. O₂ pressure is measured by solid-state fluorescent probes and converted to O₂ concentration. Every step measurement takes 5-8 min when O₂ concentration is measured every few seconds from which the OCR is calculated. Then the probes are lifted, and the larger volume of medium is mixed to restore O₂ levels to baseline conditions. Chemical compounds are injected pneumatically, limited to four sequential injections per well (Wu et al 2007).

The Oroboros O2k (Oroboros Instruments, Innsbruck, Austria) is a 2-chamber high-resolution respirometer used in cell and mitochondrial research to measure respiration in mitochondrial preparations and living cells. The O2k supports multi-sensor modules and measurement is performed in the experimental chamber, where suspended cells or mitochondrial preparations are continuously mixed by a stirrer at 750 rotations per minute. O₂ consumption in nearly diffusion-tight closed chambers is calculated in real-time from O₂ partial pressure measured by polarographic oxygen sensors. The O2k provides the option of practically unlimited titrations and, therefore, the possibility to apply various Substrate-Uncoupler-Inhibitor-Titration (SUIT) protocols designed to address specific research questions (Doerrier et al 2018; Gnaiger 2020).

2.3. Cell culture

Two human dermal fibroblast cell lines were purchased, HDF 1 (Primary Dermal Fibroblast Normal; Human, Neonatal HDFn, PCS_201_010, ATCC, NHDF-Neo), and HDF 2 (Human Dermal Fibroblasts, Neonatal, CC-2509, Lonza). A human dermal fibroblast cell line (HDF 3) was derived from a disease-free control at age of 5 months upon informed consent from General Hospital in Prague with ethics committee approval № 92/18 (18.10.2018) for project GAUK (Grant Agency of Charles University) 110119.

All cell lines were cultured in Dulbecco's modified Eagle medium (DMEM, Pan Biotech) with 25 mM glucose, 10 % fetal bovine serum and 1 % antibiotics-antimycotics 100X at 37 °C under 5 % CO₂ atmosphere. Fibroblasts cultures at passage number 13 to 15 were grown to approximately 80 % confluence. Suspended cells were counted by a Handheld Automated Cell Counter (Millipore). Cells were harvested by incubation in trypsin 0.05 % w/V with EDTA 0.02 %, w/V for 5 min at 37 °C, washed, and centrifuged at 300 *g* (5 min, 24 °C).

2.4. *Sample preparation and respirometry*

DMEM5030 was the basis of DMEM respiration medium with addition of 3.9 mM glutamate, 5 mM glucose and 2 mM pyruvate, adjusted to pH 7.4 at 37 °C. DMEM respiration medium was freshly prepared on the day of use.

Mitochondrial respiration was measured in the Agilent Seahorse XF Analyzer (XF24) according to Zhang et al (2012) with slight modifications. The day before measurement, cells were harvested, resuspended in DMEM culture medium, counted, and 35 000 cells were seeded on 20 wells of a 24-well plate for over-night incubation. 4 wells were used as blanks without cells. The plates were incubated at 5 % CO₂ atmosphere over-night and 37 °C. In parallel the Sensor Cartridge was hydrated in wells filled with Seahorse XF Calibrant Solution (Agilent) by incubation without CO₂ over-night prior to use. The XF24 was switched on during the day before experiments to equilibrate at 37 °C. On the following day, wells were washed twice with 1 mL DMEM respiration medium. 450 µL DMEM respiration medium was added to each well and incubated without CO₂ for one hour at 37 °C. In the meantime, 50 µL oligomycin (stock 20 µM; experimental concentration 2 µM) was added to cartridge port A, 55 µL FCCP (stock 5 µM) to port B, 61 µL FCCP (stock 2 µM) to port C (experimental concentrations 0.5 and 0.7 µM, respectively), and 67 µL rotenone (stock 20 µM) with antimycin A (stock 10 µM) to port D (experimental concentrations 2 and 1 µM). Sensor cartridges were incubated without CO₂ for 30-40 min at 37 °C, transferred to the XF24 for equilibration and calibration in Seahorse XF Calibrant Solution. Then the calibration well plate was exchanged for the cell plate. Before starting the respiratory protocol with living cells, wells were mixed for three min, followed by waiting for two min. Respiratory flux was measured in each state three times for three min. The transient microchamber for measurement had approximately 7 µL volume with sensors positioned 200 µm above the well bottoms.

Air calibration in the Oroboros O2k was performed daily before measurement (Gnaiger 2008). The O₂ partial pressure for air calibration is calculated (DatLab software) for air saturated 100 % with water vapor at experimental temperature and local barometric pressure recorded real-time by the electronic pressure transducer of the O2k. The O₂ solubility of DMEM respiration medium was assumed to be 92 % relative to the O₂ solubility of pure water at 37 °C (Gnaiger 2021a). Calibrations at zero O₂ concentration were performed before experimental series. Instrumental O₂ background flux (Gnaiger 2001) was measured each day before the experiment with cells in the range of O₂ concentration from air saturation at 180 µM to 100 µM.

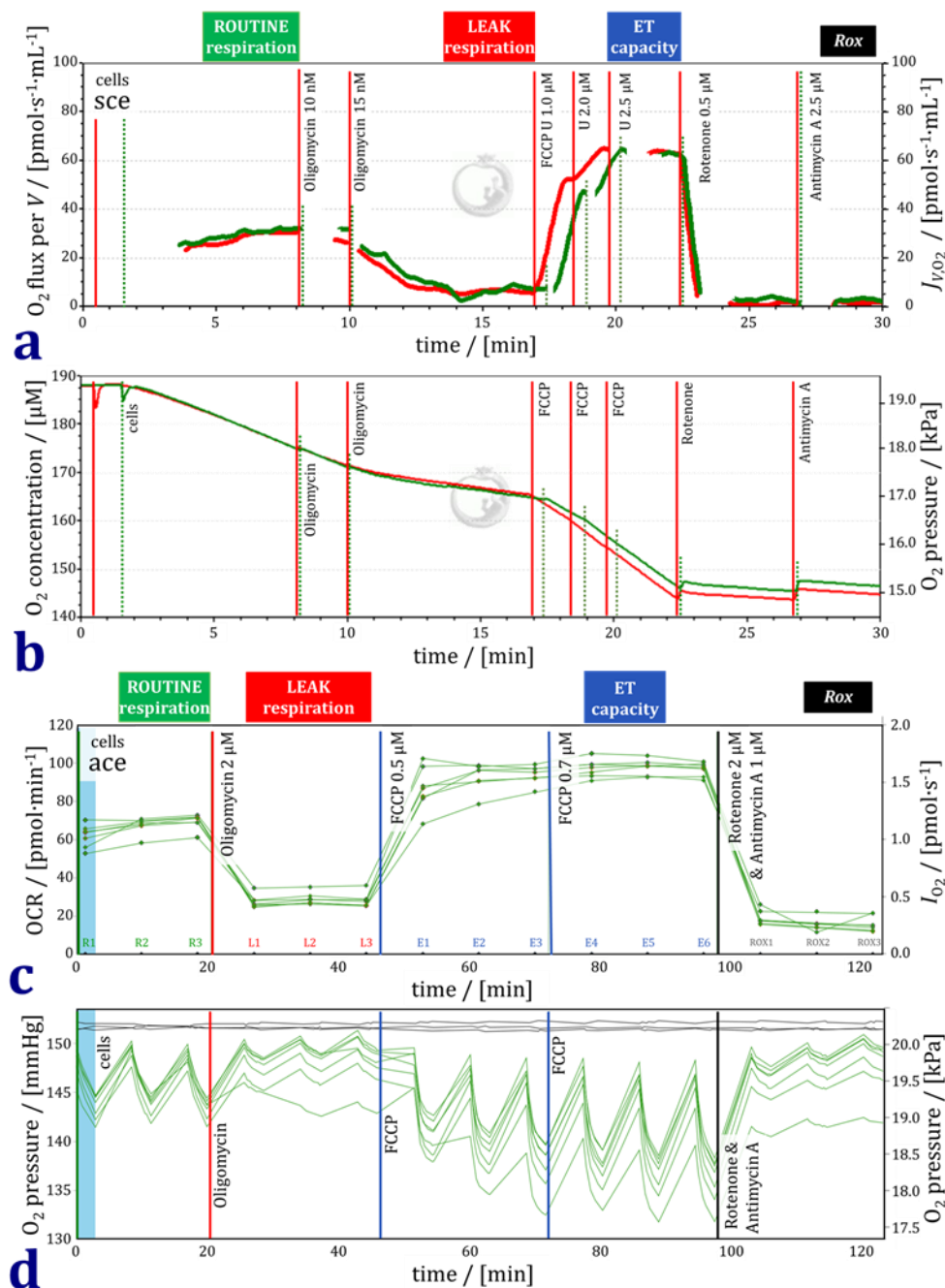


Figure 1. Representative traces of respiration and O_2 concentration or O_2 pressure in the protocol with living human dermal fibroblasts (HDF 1). (a) O_2 flux per volume in two chambers measured simultaneously in the Oroboros O2k. (b) O_2 concentration and partial O_2 pressure corresponding to the traces in panel a. (c) O_2 consumption rate (OCR) measured simultaneously in six wells of one plate of the XF24. Three time-intervals of respiration per respiratory state (R1, R2, R3; L1, L2, L3; etc.). (d) O_2 partial pressure corresponding to the traces in panel c.

2.5. Respiratory protocols

Comparable respiratory protocols were used with the Agilent XF24 and Oroboros O2k using the same DMEM respiration medium (Figure 1). Every cell line was measured on the same day in parallel, splitting the cells from one culture flask into two O2k-chambers and 20 wells of the XF24. In the coupling control protocol for living cells (SUIT-003), four respiratory states are distinguished (Hütter et al 2004). We adhere to the platform-independent terminology of the MitoEAGLE consensus paper (Gnaiger et al 2020) and add the terms widely used in conjunction with the XF24 or XF96 (Zhang et al 2012) in parentheses. First, ROUTINE respiration R ('basal respiration') was measured in attached or suspended cells. The ROUTINE state is a physiological state, in which respiration is controlled by cellular energy demand. Next, the ATP synthase inhibitor oligomycin was added to induce LEAK respiration L ('proton leak'). In the non-phosphorylating LEAK state, a low rate of respiration is maintained mainly to compensate for the proton leak at a high protonmotive force. Afterwards, the uncoupler FCCP was titrated in at least two steps to obtain a maximum rate of O_2 consumption reflecting the electron transfer capacity E ('maximal respiration') in the noncoupled state. Finally, antimycin A and rotenone were added. These inhibitors of Complexes CI and CIII, respectively, inhibit mitochondrial electron transfer and thus induce residual oxygen consumption Rox ('nonmitochondrial respiration') due to oxidative side reactions. Importantly, the plasma membrane is permeable for these inhibitors and the uncoupler which, therefore, can be applied in living cells. The concentrations applied in the XF24 and O2k adhered closely to the respective manuals (Figure 1; Table S1).

2.6. Data analysis

Measurements were normalized for the cell count. Traces were analyzed in DatLab 7 software (Oroboros Instruments) where each O2k-chamber contained 375 000 cells. O_2 flow is expressed per cell [$\text{amol}\cdot\text{s}^{-1}\cdot\text{x}^{-1}$] equivalent to [$\text{pmol}\cdot\text{s}^{-1}\cdot(10^6 \text{ x})^{-1}$]. The Wave 2 software (Agilent) presents results in units [$\text{pmol}\cdot\text{min}^{-1}$] in a well which contained 35 000 cells. Data were converted to the same units [$\text{amol}\cdot\text{s}^{-1}\cdot\text{x}^{-1}$], where x represents the unit cell (Gnaiger et al 2020; Gnaiger 2021b). In regressions between respiration for different states, variables in X and Y have comparable errors of measurement. To minimize the residuals of both variables, Y and X , slopes b_Y and β_X and intercepts a_Y and α_X are calculated for the Y/X and X/Y inverted linear regressions, respectively. The mean slope $\bar{b} = (b_Y + b_X)/2$ and mean intercept $\bar{a} = (a_Y + \alpha_X)/2$ are used, where $b_X = 1/\beta_X$ and $a_X = -\alpha_X/\beta_X$ (Gnaiger 2021c). Further statistical evaluation was performed using GraphPad Software (California, USA). Rox -corrected rates were symmetrically distributed, and logarithmic transformation was not required. One outlier was removed in the XF24 with negative LEAK respiration irrespective of Rox -correction. There were no outliers in the O2k.

3. Results

3.1. Respiration normalized for cell count

Respiratory rates measured in the XF24 (ace) and O2k (sce) are expressed per cell in units for O_2 flow [$\text{amol}\cdot\text{s}^{-1}\cdot\text{x}^{-1}$] and shown on identical scales in Figures 2a and b. The ranking of respiratory capacities of the three cell lines followed different patterns in the XF24 and O2k, which is taken as an argument for pooling all results in the scatter plots. The variability within cell lines was greater in the XF24 ($n=20$) than the O2k ($n=4$). Averaging five wells of the XF24 to obtain $n = 4$ per cell line did not reduce the coefficient of variation (SD/average), which was 0.29 and 0.26 for *R* and *E* ($n=20$) to 0.27 and 0.27 ($n=4$, each for 5 pooled wells), compared to the coefficient of variation of 0.10 and 0.10 for *R* and *E* in the O2k (Table 1a).

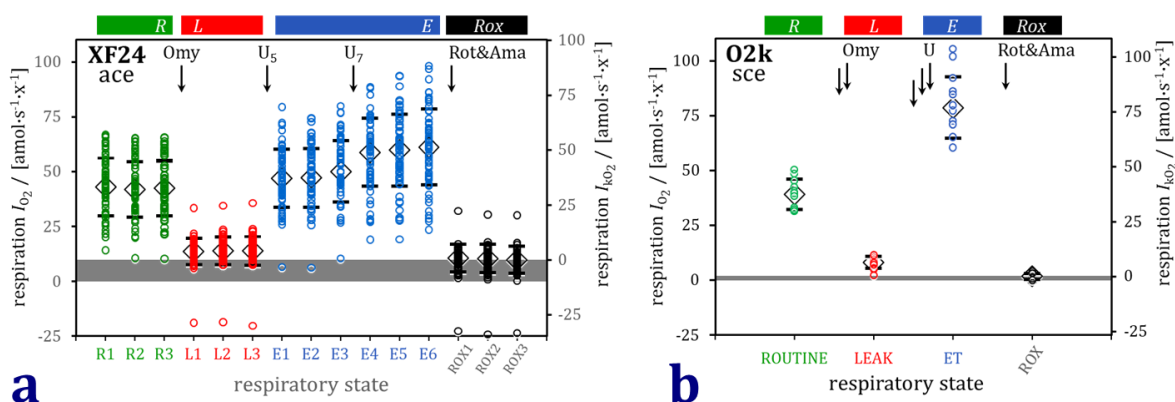


Figure 2. Sequence of respiratory states in the coupling control protocol applied in the XF24 for ace (a) and O2k for sce (b). Circles: individual wells or chambers; diamonds and bars: median \pm SD. ROUTINE respiration *R*; LEAK respiration *L*; electron transfer capacity *E*; residual oxygen consumption *Rox*.

Rates of O_2 consumption are expected to be identical in adherent and suspended cells in the LEAK, ET, and ROX states when physiological control of cellular energy demand is eliminated. This is achieved by inhibition of mitochondrial electron transfer using rotenone and antimycin A blocking Complex I and III, respectively, and thus inducing the state of residual oxygen consumption ROX. Similarly, inhibition of ATP synthase by oligomycin induces LEAK respiration *L* in a state that is not controlled by cellular ATP turnover. ROX and LEAK are, therefore, states of minimum O_2 consumption providing a comparison of instrumental resolution of the two instrument types, independent of using attached cells (ace) in the XF24 and suspended cells (sce) in the O2k. Residual oxygen consumption *Rox* and total LEAK respiration L'_{tot} not corrected for *Rox* were higher with a larger scatter in the XF24 (ace) compared to the O2k (sce) (Figures 3a and b). *Rox*-correction of LEAK respiration *L*, however, eliminated the differences observed in the two platforms (Figure 3c). Bioenergetic cluster analysis BCA (Gnaiger 2021c) shows the pairwise correlation between *Rox* and total LEAK respiration (Figures 3d and e).

ROUTINE respiration R is under physiological control of living cells. Therefore, R reflects the possible changes in mitochondrial ATP demand induced by suspending cells that are grown attached in the monolayer. R_{ox} -corrected R was similar in attached cells measured in the XF24 and suspended cells measured in the O2k (Figure 3f).

Electron transfer capacity E is supported by physiological substrates in the living cell but is entirely independent of respiratory control by cellular ATP demand. Therefore, E corrected for R_{ox} was expected to be independent of cell physiology and comparable in suspended and attached cells. However, E was lower in ace than sce (Figure 3g). Results for the three cell lines are summarized in Table 1a.

Table 1. Respiration of three human fibroblast cell lines attached (ace; XF24) or suspended (sce; O2k). Median \pm SD. (a) R , L and E corrected for residual oxygen consumption R_{ox} . n are technical repeats. (b) Flux control ratios and flux control efficiencies normalized for ET capacity as an internal normalization to express respiration independent of cell count. R_{ox} was normalized for total O_2 consumption E'_{tot} in the noncoupled state. E'_{tot} was determined immediately before inhibition by antimycin A and is the electron transfer capacity without correction for R_{ox} .

a					
Cell line	Number of repeats n or groups	ROUTINE R [$\mu\text{mol}\cdot\text{s}^{-1}\cdot\text{x}^{-1}$]	LEAK L [$\mu\text{mol}\cdot\text{s}^{-1}\cdot\text{x}^{-1}$]	ET capacity E [$\mu\text{mol}\cdot\text{s}^{-1}\cdot\text{x}^{-1}$]	R_{ox} [$\mu\text{mol}\cdot\text{s}^{-1}\cdot\text{x}^{-1}$]
ace ₁	$n = 20$	33 ± 5	5 ± 2	51 ± 7	8 ± 8
ace ₂	$n = 20$	39 ± 10	6 ± 2	60 ± 14	11 ± 6
ace ₃	$n = 19$	30 ± 13	5 ± 2	44 ± 18	7 ± 4
sce ₁	$n = 4$	45 ± 4	7 ± 1	94 ± 9	2 ± 1
sce ₂	$n = 4$	35 ± 4	6 ± 3	75 ± 7	1 ± 2
sce ₃	$n = 4$	31 ± 3	3 ± 1	69 ± 7	2 ± 2
ace _{mean}	$N = 3$	34 ± 4	5 ± 1	52 ± 8	9 ± 2
sce _{mean}	$N = 3$	37 ± 7	6 ± 2	79 ± 13	2 ± 1
b					
Cell line	Number of replica n or groups N	control ratio R/E	net R/E ratio $(R-L)/E$	net E ratio $(E-L)/E$	ROX R_{ox}/E'_{tot}
ace ₁	$n = 20$	0.64 ± 0.07	0.56 ± 0.06	0.91 ± 0.06	0.14 ± 0.27
ace ₂	$n = 20$	0.61 ± 0.10	0.56 ± 0.11	0.89 ± 0.04	0.15 ± 0.08
ace ₃	$n = 19$	0.71 ± 0.07	0.60 ± 0.08	0.92 ± 0.07	0.15 ± 0.06
sce ₁	$n = 4$	0.46 ± 0.04	0.38 ± 0.04	0.92 ± 0.00	0.02 ± 0.01
sce ₂	$n = 4$	0.49 ± 0.06	0.39 ± 0.03	0.91 ± 0.04	0.01 ± 0.02
sce ₃	$n = 4$	0.45 ± 0.04	0.41 ± 0.02	0.96 ± 0.02	0.03 ± 0.02
ace _{mean}	$N = 3$	0.61 ± 0.05	27.4 ± 4.7	0.90 ± 0.03	0.16 ± 0.01
sce _{mean}	$N = 3$	0.47 ± 0.02	31.2 ± 5.9	0.93 ± 0.03	0.02 ± 0.01

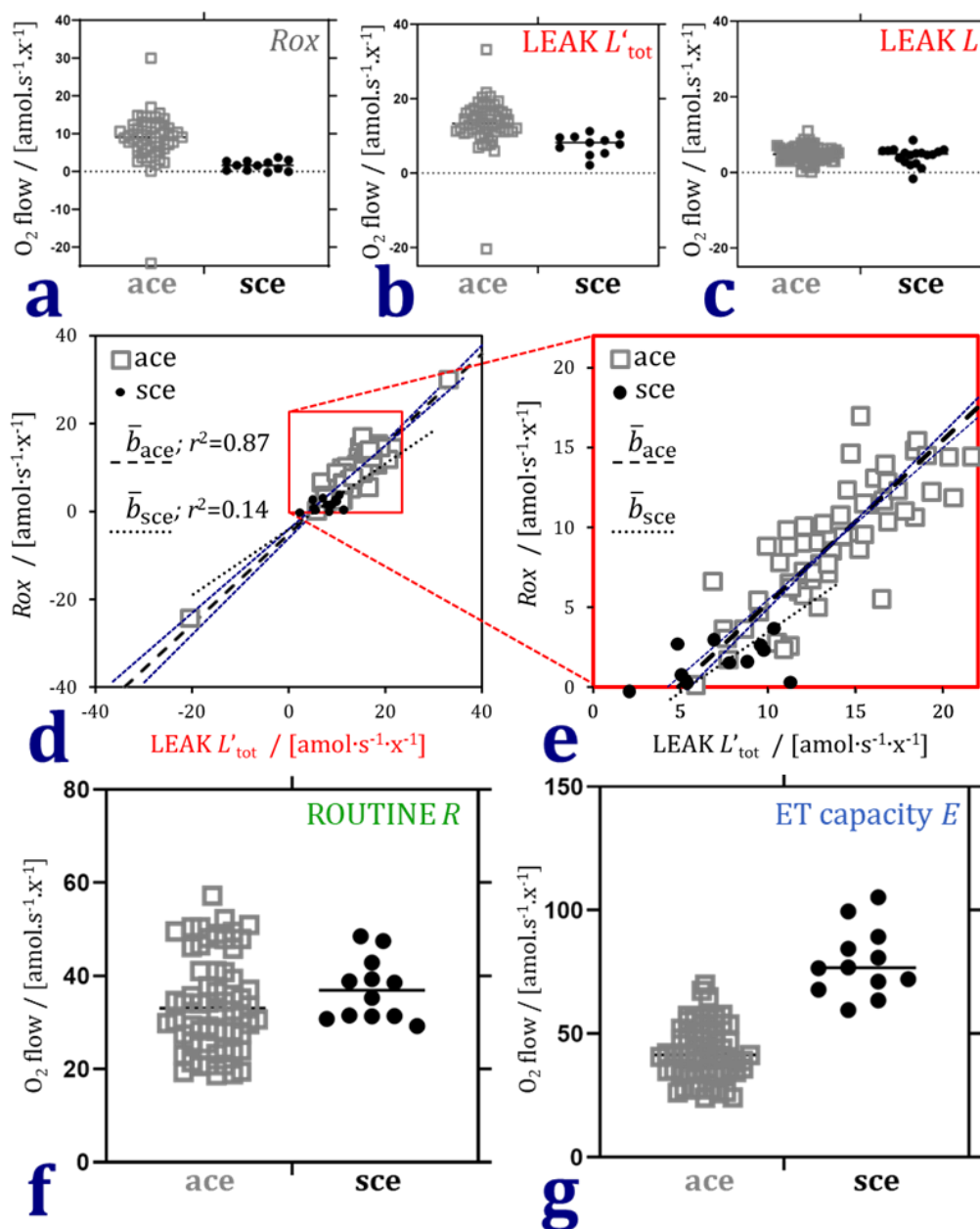


Figure 3. Residual oxygen consumption Rox , LEAK respiration L , ROUTINE respiration R , and electron transfer capacity E in attached and suspended fibroblast cells (ace and sce). (a) Rox measured after inhibition by rotenone and antimycin A reflects instrumental resolution independent of cell physiological conditions for comparison of the two respirometers (ace: XF24, sce: O2k). (b) Total LEAK respiration L'_{tot} uncorrected for Rox , higher in ace than sce. (c) Rox -correction of LEAK respiration L eliminates the difference between ace and sce. (d) Relation between Rox and L'_{tot} (full range). \bar{b} is the mean slope of the ordinate and inverted slopes which are shown for ace (thin dashed lines). The low coefficient of determination r^2 for sce is related to the very low scatter of the data. (e) Zoom into the positive range of values in panel d. (f) Rox -corrected ROUTINE respiration was similar in ace and sce. (g) Rox -corrected electron transfer capacity was lower in ace than sce.

3.2. ROUTINE versus LEAK respiration and electron transfer capacity

Internal normalization eliminates any possible bias caused by methodological differences in determining the concentration of cells per experimental chamber volume in wells (attached; ace) and in suspension (sce).

ET capacity is frequently used as a reference and functional mt-marker (Table 1b). The higher R/E flux control ratio in ace, however, does not indicate a lower ROUTINE respiration in sce, which would contradict results on O_2 flow normalized for cell count (Figure 3). BCA illustrates a left shift of the R/E regression line due to lower ET capacity in ace compared to sce, at comparable ROUTINE respiration of suspended and attached cells (Figure 4a). The compensatory increase of R as a function of intrinsic uncoupling detected by increasing L in sce (Figure 4b) conforms to a pattern generally observed in cell respiration (Gnaiger 2021c). Noise in the ace data prevents resolution, yet the overlap of clusters supports the conclusion based on O_2 flow (Figure 3f) that ROUTINE respiration was not different in ace and sce.

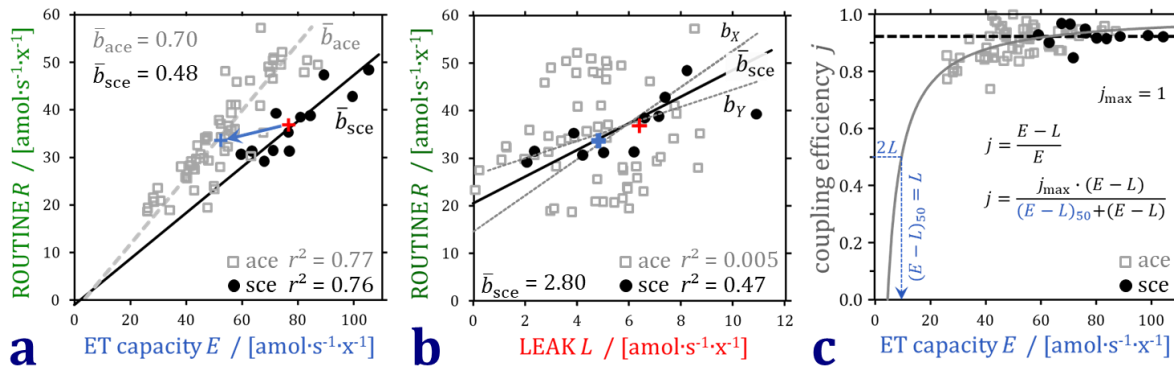


Figure 4. Bioenergetic cluster analysis of respiration in different respiratory coupling states in attached and suspended cells (ace and sce). (a) R varies in direct proportion to ET capacity. The linear R/E regressions are different for ace and sce, thus the data points are arranged as separate heterolinear clusters with different \bar{b}_{ace} and \bar{b}_{sce} . E is lower in ace than sce at similar R (blue arrow pointing to the left from the median of sce to the median of ace). (b) ace and sce are in the same cluster in the plot of R versus L , with high noise in ace LEAK respiration. For sce, b_y and b_x indicate the slopes for the ordinary and inverted least squares regressions. The trend of R increasing linearly with L and a positive intercept agree with results on different human fibroblasts (Gnaiger 2021c). (c) A constant coupling control efficiency j at declining E (dotted line for sce) is predicted at constant mitochondrial quality with proportional decline of E and L . The relationship between coupling efficiency and E at constant L is hyperbolic (full line fitted for ace). $(E-L)_{50}$ is the net ET capacity when coupling efficiency is 50%. The maximum coupling efficiency, $j_{max} \stackrel{def}{=} 1$, is approached with increasing E .

Low ET capacities in ace are explained by (1) the high oligomycin concentration applied in the XF24 compared with the minimum oligomycin concentration optimized by titrations in each experiment conducted in the O2k and (2) low uncoupler concentrations and a trend suggesting further increase of O_2 flow in the ET state (Figure 2a).

Declining E at constant L lowers the $E-L$ coupling efficiency, $j = (E-L)/E$, by an ET-linked mechanism. The distinction between ET-linked and uncoupling-linked effects,

however, is not apparent from the ratios presented in [Table 1b](#). When E and L are expressed as O_2 flow per cell ([Table 1a](#)) and vary proportionally due to differences in cell size, mt-density, and noise in the cell count, then coupling efficiency remains constant at variable ET capacity, as seen in [sce](#) ([Figure 4c](#)). Even when E is underestimated progressively, the drop in $(E-L)/E$ is small initially, since the decline in $(E-L)$ is partially compensated for by the decline of E . The relationship between coupling efficiency and declining E at constant L is hyperbolic. The XF24 data follow this nonlinear model as a separate cluster overlapping with the O2k data at high coupling efficiency ([Figure 4c](#)).

4. Discussion

Cells cultured attached to a physical substrate undergo many changes when they are detached and maintained in suspension, but possible bioenergetic respiratory changes have not yet been addressed. Suspending fibroblasts causes an immediate drop of mRNA synthesis to about 20 % of controls within minutes (Benecke et al 1978). The remaining mRNA is inactivated, such that the total cell mRNA content remains unchanged. The rate of protein labeling declines more slowly, even slower than expected from the mRNA lifetime of about nine hours (Abelson et al 1974). Nevertheless, the suspended cells contain – after almost 3 days of reduced messenger RNA production – unchanged levels of cytoplasmic polyadenylated RNA due to a stabilization of mRNA against normal turnover. A continuous decline in protein synthesis starts after 12 h in suspension (Benecke et al 1978). The recovery of protein synthesis is rapid after reattachment of cells to a tissue culture dish and reactivation of the sequestered mRNA (Ben-Ze'ev et al 1990). These responses of cells to suspension or attachment suggest the possibility of inducing metabolic responses by altered physical configuration and cell morphology (Benecke et al 1978). To our knowledge, the bioenergetic consequences of suspending fibroblasts grown in a monolayer have not yet been quantitatively assessed, despite numerous studies reporting fibroblast respiration of either suspended or attached cells. Our results suggest that ROUTINE respiration was not different in attached cells studied after overnight seeding and freshly suspended cells measured one hour after harvesting. These findings are relevant for interpreting respirometric short-term studies, but do not exclude severe bioenergetic alterations and even cell death as a consequence of prolonged suspension of fibroblasts. Importantly, cells do not immediately change their configuration when re-plated after trypsinization (Benecke et al 1980).

For comparison of respiration of attached and suspended fibroblasts it was necessary to use two different platforms, on one hand multiwell microchambers containing attached cells without stirring, and on the other hand 0.5-mL twin chambers that are stirred continuously to maintain cells in homogenous suspension and to avoid O_2 diffusion gradients which would compromise high-resolution respirometry. Primarily, therefore, the quantitative agreement of measurements with the two instruments had to be evaluated. Higher rates of residual oxygen consumption Rox and total LEAK respiration not corrected for Rox were obtained in the XF24. This may be attributed to variable instrumental background rather than the attached state of the cells, which is supported by the fact that Rox -corrected LEAK respiration was not different in [ace](#) and [sce](#).

Our results can be compared with a large database on respiration of normal human dermal fibroblasts NHDF measured with the Seahorse XF96 Analyzer and used as controls for the diagnosis of inherited mitochondrial diseases (Yépez et al 2018). NHDF data from 2630 wells are summarized in a meta-analysis based on BCA (Gnaiger 2021c). Respiration was normalized for the count of seeded cells (20 000 cells per well in the XF96, compared to 35 000 cells per well in the XF24 and 375 000 cells in the O2k chamber in the present study). After (1) conversion of the NHDF raw data to SI units, (2) deletion of runs with missing data points, (3) further elimination of 7 % of outliers (Yépez et al 2018 report 17 % outliers), and (4) log transformation to account for positive skewness, the NHDF data are expressed as means \pm SD after linear back-transformation. R , L and E are 37 ± 12 ; 6 ± 3 ; and 78 ± 26 $\text{amol}\cdot\text{s}^{-1}\cdot\text{x}^{-1}$, respectively (Gnaiger 2021c). This agrees with our results on suspended cells in the O2k and attached cells in the XF24 for R and L (Table 1). Our data on E in the XF24 after $2 \mu\text{M}$ oligomycin and uncoupler titration up to $0.7 \mu\text{M}$ were lower (52 ± 8) compared to 78 ± 25 in the XF96 at a lower oligomycin concentration ($1 \mu\text{M}$) and higher FCCP concentration ($1 \mu\text{M}$; Yépez et al 2018). This supports the interpretation, that ET capacity was underestimated in the present study in the XF24 due to an insufficiently high uncoupler concentration (Figure 2a) combined with a high concentration of oligomycin inhibiting E .

Taken together, neither LEAK respiration nor ROUTINE respiration were different comparing attached and suspended cells. BCA identified the lower coupling control efficiency obtained in the XF24 as being caused by underestimation of ET capacity as opposed to uncoupling (Figure 4c). Further studies of respiration in different attached and suspended cell types are of great interest in cell physiology, particularly in neuronal cells and blood cells. The present approach includes bioenergetic cluster analysis and provides a guideline for extending databases on cell respiration across instrumental platforms, emphasizing the importance of harmonization of protocols.

Acknowledgements

This work was partially funded by the European Union's Horizon 2020 research and innovation programme under grant agreement No. 859770, NextGen-O2k project, and by Institutional project GAUK110119. Contribution to COST Action CA15203 MitoEAGLE with financial support of Short-Term Scientific missions (LD).

Abbreviations

amol	attomole (10^{-18} moles)
ace	attached cells
DMEM	Dulbecco's modified Eagle's medium
E and E'_{tot}	ET capacity per cell, <i>Rox</i> -corrected and total [$\text{amol}\cdot\text{s}^{-1}\cdot\text{x}^{-1}$]
$(E-L)_{50}$	net ET capacity when coupling efficiency is 50 % in the hyperbolic dyscapacity model; $(E-L)_{50} = L$; $E_{50} = 2\cdot L$
EDTA	Ethylenediaminetetraacetic acid
ETS	electron transfer system
FCCP	Carbonyl cyanide 4-(trifluoromethoxy)phenylhydrazone
HRR	high-resolution respirometry
I_{O_2}	O ₂ flow per cell count

j	coupling control efficiency $(E-L)/E$
j_{\max}	maximum coupling control efficiency, by definition $j_{\max} \stackrel{\text{def}}{=} 1$
J_{O_2}	O ₂ flux per chamber volume
L and L'_{tot}	LEAK respiration per cell, <i>Rox</i> -corrected and total [$\text{amol}\cdot\text{s}^{-1}\cdot\text{x}^{-1}$]
M	mega (10^6)
M	molar ($\text{mol}\cdot\text{L}^{-1}$)
mt	mitochondria(l)
n	number of technical repeats or total number of measurements
N	number of independent replica
N_{ce}	cell count, number of cells [x]
OCR	oxygen consumption rate
p	pico (10^{-12})
R and R'_{tot}	ROUTINE respiration per cell, <i>Rox</i> -corrected and total [$\text{amol}\cdot\text{s}^{-1}\cdot\text{x}^{-1}$]
ROX	residual oxygen consumption state
<i>Rox</i>	residual oxygen consumption (per cell [$\text{amol}\cdot\text{s}^{-1}\cdot\text{x}^{-1}$])
sce	suspended cells
SUIT	substrate-uncoupler-inhibitor titration
TE	trypsin 0.05 % w/V with EDTA 0.02 %, w/V
U	uncoupler
x	elementary unit

References

- Abelson HT, Johnson LF, Penman S, Green H (1974) Changes in RNA in relation to growth of the fibroblast: II. The lifetime of mRNA, rRNA, and tRNA in resting and growing cells. *Cell* 1:161-5. doi.org/10.1016/0092-8674(74)90107-X
- Benecke BJ, Ben-Ze'ev A, Penman S (1978) The control of mRNA production, translation and turnover in suspended and reattached anchorage-dependent fibroblasts. *Cell* 14:931-9. doi.org/10.1016/0092-8674(78)90347-1
- Benecke BJ, Ben-Ze'ev A, Penman S (1980) The regulation of RNA metabolism in suspended and reattached anchorage-dependent 3T6 fibroblasts. *J Cellular Physiol* 103:247-54. doi.org/10.1002/jcp.1041030209
- Ben-Ze'ev A, Reiss R, Bendori R, Gorodecki B (1990) Transient induction of vinculin gene expression in 3T3 fibroblasts stimulated by serum-growth factors. *Cell Regulation* 1:621-6. doi.org/10.1091/mbc.1.9.621
- Farmer SR, Ben-Ze'ev A, Benecke BJ, Penman S (1978) Altered translatability of messenger RNA from suspended anchorage-dependent fibroblasts: reversal upon cell attachment to a surface. *Cell* 15:627-37. doi.org/10.1016/0092-8674(78)90031-4
- Doerrier C, Garcia-Souza LF, Krumschnabel G, Wohlfarter Y, Mészáros AT, Gnaiger E (2018) High-Resolution FluoRespirometry and OXPHOS protocols for human cells, permeabilized fibers from small biopsies of muscle, and isolated mitochondria. *Methods Mol Biol* 1782:31-70. doi.org/10.1007/978-1-4939-7831-1_3
- Gnaiger E (2001) Bioenergetics at low oxygen: dependence of respiration and phosphorylation on oxygen and adenosine diphosphate supply. *Respiration Physiol* 128:277-97. doi.org/10.1016/s0034-5687(01)00307-3
- Gnaiger E (2008) Polarographic oxygen sensors, the oxygraph and high-resolution respirometry to assess mitochondrial function. In: *Mitochondrial dysfunction in drug-induced toxicity*

- (Dykens JA, Will Y, eds) John Wiley & Sons, Inc, Hoboken, NJ:327-52. doi.org/10.1002/9780470372531.ch12
- Gnaiger E (2020) Mitochondrial pathways and respiratory control. An introduction to OXPHOS analysis. 5th ed. Bioenerg Commun 2020.2: 112 pp. doi:10.26124/bec:2020-0002
- Gnaiger E et al – MitoEAGLE Task Group (2020) Mitochondrial physiology. Bioenerg Commun 2020.1:1-44. doi:10.26124/bec:2020-0001.v1
- Gnaiger E (2021a) O2k Quality Control 1: Polarographic oxygen sensors and accuracy of calibration. Mitochondr Physiol Network 06.03(19):1-19. – https://wiki.oroboros.at/index.php/MiPNet06.03_POS-calibration-SOP
- Gnaiger E (2021b) The elementary unit — canonical reviewer's comments on: Bureau International des Poids et Mesures (2019) The International System of Units (SI) 9th ed. MitoFit Preprints 2020.4.v2. doi:10.26124/mitofit:200004.v2
- Gnaiger E (2021c) Bioenergetic cluster analysis – mitochondrial respiratory control in human fibroblasts. MitoFit Preprints 2021.8. doi.org/ 10.26124/mitofit:2021-0008
- Harrison CJ, Allen TD (1979) Cell surface morphology after trypsinisation depends on initial cell shape. Differentiation 15:61-6. doi.org/10.1111/j.1432-0436.1979.tb01035.x
- Hütter E, Renner K, Pfister G, Stöckl P, Jansen-Dürr P, Gnaiger E (2004) Senescence-associated changes in respiration and oxidative phosphorylation in primary human fibroblasts. Biochem J 380:919–28. doi.org/10.1042/BJ20040095
- Lazdins JK, Koech DK, Karnovsky ML (1980) Oxidation of glucose by mouse peritoneal macrophages: a comparison of suspensions and monolayers. J Cellular Physiol 105:191–6. doi.org/10.1002/jcp.1041050202
- Park JY, Jeong AL, Joo HJ, Han S, Kim SH, Kim HY, Lim JS, Lee MS, Choi HK, Yang Y (2017) Development of suspension cell culture model to mimic circulating tumor cells. Oncotarget 9:622–40. doi.org/10.18632/oncotarget.23079
- Pofit JF, Strauss PR (1977) Membrane transport by macrophages in suspension and adherent to glass. J Cellular Physiol 92:249–55. doi.org/10.1002/jcp.1040920213
- Shen CF, Guilbault C, Li X, Elahi SM, Ansoorge S, Kamen A, Gilbert R (2019) Development of suspension adapted Vero cell culture process technology for production of viral vaccines. Vaccine 37:6996–7002. doi.org/10.1016/j.vaccine.2019.07.003
- Wu M, Neilson A, Swift AL, Moran R, Tamagnine J, Parslow D, Armistead S, Lemire K, Orrell J, Teich J, Chomicz S, Ferrick DA (2007) Multiparameter metabolic analysis reveals a close link between attenuated mitochondrial bioenergetic function and enhanced glycolysis dependency in human tumor cells. Am J Physiol Cell Physiol 292:C125–36. doi.org/10.1152/ajpcell.00247.2006
- Yépez VA, Kremer LS, Iuso A, Gusic M, Kopajtich R, Koňářková E, Nadel A, Wachutka L, Prokisch H, Gagneur J (2018) OCR-Stats: robust estimation and statistical testing of mitochondrial respiration activities using Seahorse XF Analyzer. PLOS ONE 13:e0199938. doi.org/10.1371/journal.pone.0199938
- Zhang J, Nuebel E, Wisidagama DR, Setoguchi K, Hong JS, Van Horn CM, Imam SS, Vergnes L, Malone CS, Koehler CM, Teitell MA (2012) Measuring energy metabolism in cultured cells, including human pluripotent stem cells and differentiated cells. Nature Protocols 7:1068–85. doi.org/10.1038/nprot.2012.048

Copyright: © 2021 The authors. This is an Open Access preprint (not peer-reviewed) distributed under the terms of the Creative Commons Attribution License, which permits unrestricted use, distribution, and reproduction in any medium, provided the original authors and source are credited. © remains with the authors, who have granted MitoFit Preprints an Open Access publication license in perpetuity.



Supplements

Supplement 1. Mitochondrial respiratory coupling states of living cells

When respiratory rate or oxygen consumption rate OCR is expressed for a defined experimental chamber (O2k-chamber; XF-well), then O₂ flow I_{O_2} [pmol·s⁻¹] depends on the cell count N_{ce} [10^6 x] = [Mx] in the experimental chamber or on the cell concentration and chamber volume. OCR represented as O₂ flow I_{O_2} in a chamber cannot be compared across experiments with variable N_{ce} (Gnaiger et al 2020). Comparability of respiration between identical cells in a given respiratory state (such as ROUTINE respiration R) is achieved by normalization for N_{ce} , $R = I_R \cdot N_{ce}^{-1}$ [pmol·s⁻¹·(10⁶ x)⁻¹] = [amol·s⁻¹·x⁻¹].

Table S1. Harmonization of terminology on respiratory states. Comparison of platform-independent MitoEAGLE terms (Gnaiger et al 2020) and terms frequently used in the context of Seahorse XF Analyzer applications (Agilent Technologies 2019). R , L , and E are baseline-corrected for R_{ox} .

	MitoEAGLE Task Force 2020	Seahorse XF Analyzer	Definition
R	ROUTINE respiration	basal respiration	physiological respiration controlled by cellular energy demand, energy turnover and the degree of coupling to phosphorylation
L	LEAK respiration	proton LEAK	non-phosphorylating state, respiration maintained mainly to compensate for the proton leak at a high chemiosmotic potential
E	electron transfer capacity	maximal respiration	oxygen consumption with a short circuit of the H ⁺ cycle across the mitochondrial inner membrane stimulating maximum O ₂ flux
R_{ox}	residual oxygen consumption	nonmitochondrial respiration	respiration due to oxidative side reactions in the ROX-state after Complex I and III inhibition

Supplement 2. Uncoupler and inhibitor concentrations

Table S2. Recommended and applied experimental concentrations of inhibitors and uncoupler.

	Compound	Gnaiger (2020)	O2k applied	Agilent (2019)	XF24 applied
<i>L</i>	Oligomycin	5-10 nM titration steps	10–15 nM	0.5–2.5 μ M	2 μ M
<i>E</i>	FCCP	0.5 μ M titration steps CCCP	2–2.5 μ M FCCP	0.125–2.0 μ M FCCP	0.7 μ M FCCP
<i>Rox</i>	Rotenone	0.5 μ M	0.5 μ M	0.5 μ M	2 μ M
	Antimycin A	2.5 μ M	2.5 μ M	0.5 μ M	1 μ M

References

- Agilent Technologies (2019) Mito Stress Test Kit, User Guide. Available: [https://www.agilent.com/cs/library/usermanuals/public/XF_Cell_Mito Stres...](https://www.agilent.com/cs/library/usermanuals/public/XF_Cell_Mito_Stres...)
- Gnaiger E (2020) Mitochondrial pathways and respiratory control. An introduction to OXPHOS analysis. 5th ed. Bioenerg Commun 2020.2: 112 pp. doi:10.26124/bec:2020-0002
- Gnaiger E et al – MitoEAGLE Task Group (2020) Mitochondrial physiology. Bioenerg Commun 2020.1:1-44. doi:10.26124/bec:2020-0001.v1